

Programming 3D curves with discretely constrained cylindrical inflatables

Robert Baines^a, Sree Kalyan Patiballa^{a,b}, Benjamin Gorissen^{c,d}, Katia Bertoldi^c, and Rebecca Kramer-Bottiglio^{a,1}

^aYale University; ^bThe University of Alabama; ^cHarvard University; ^dKU Leuven

This manuscript was compiled on March 27, 2023

1 **Programming inflatable systems to deform to desired three-**
2 **dimensional (3D) shapes opens up multifarious applications in**
3 **robotics, morphing architecture, and interventional medicine. This**
4 **work elicits complex deformations by attaching discrete strain lim-**
5 **iters to cylindrical hyperelastic inflatables. Using this system, we**
6 **present a method to solve the inverse problem of programming myri-**
7 **ad 3D centerline curves upon inflation. The method entails two**
8 **steps: first, a reduced-order model generates a conceptual solution**
9 **giving coarse indications of strain limiter placement on the unde-**
10 **formed cylindrical inflatable. This low-fidelity solution then seeds**
11 **a finite element simulation nested within an optimization loop to fur-**
12 **ther tune strain limiter parameters. We leverage this framework to**
13 **achieve functionality through *a-priori* programmed deformations of**
14 **cylindrical inflatables, including 3D curve matching, self-tying knot-**
15 **ting, and manipulation. Results hold broad significance for the**
16 **emerging computational design of inflatable systems.**

soft robotics | soft actuators | inflatables | programmable matter | inverse design

1 **T**he potential of inflatable systems to assume complex
2 shapes and interact adaptively with their environment
3 has propelled them to the forefront of next-generation soft
4 robotics, deployable structures, and medical devices (1–3).
5 Critical interest has thus emerged regarding the inverse design
6 of inflatables and other volumetrically expanding systems—
7 specifying a deformation, and solving for the design param-
8 eters, *i.e.* geometric and/or material parameters, required
9 to achieve this deformation (4–6). Inverse design can reduce
10 prototyping time, material waste, and results in more per-
11 formant soft systems. Many inverse inflatable models have
12 focused on systems composed of materials with a high elastic
13 modulus (making quasi-inextensible at operating pressure).
14 This hardware choice reduces the modeling challenge yet limits
15 the scope of achievable deformations (7–10).

16 Inflatables composed of hyperelastic material can accom-
17 modate large strains, disposing them to applications requiring
18 radical shape changes or large forces (11, 12). Hyperelas-
19 tic inflatables commonly incorporate stiffer material strain
20 limiters, including mesh, directional fibers, slotted shells, or
21 varying-modulus rubber on their surface to direct deformations
22 (13–17). Simpler deformations like contraction or extension are
23 well-studied and can be designed *a-priori* with reduced force
24 or energy-based models (18–20). Models like these assume
25 homogeneous deformations throughout the system, induced
26 by a single strain limiter on an inflatable undergoing typically
27 small (<40%), planar, and axisymmetric deformations. Sim-
28 ilarly, models for specification of curvatures are capable of
29 programming only planar curves and have been demonstrated
30 with unidirectionally extending cylinders (21).

31 Deformable systems that can inflate into non-homogeneous
32 3D forms open a more expansive application space. In these

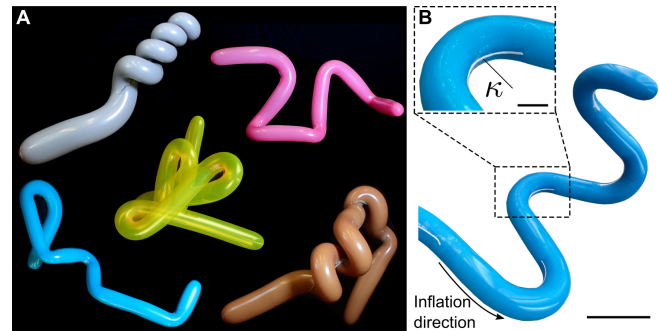


Fig. 1. Adhering discrete strain-limiting patches to the surface of hyperelastic inflatable cylinders gives rise to complex and functional forms. A. Several inflatables fabricated using this technique are shown. B. Image of prototype inflatable with patches that influence curvature κ and torsion τ in extremely non-linear ways based on their dimensions, orientation, and placement along the continuum surface. The zoomed inset shows how even a localized 1 mm-wide, 4 cm long patch can produce curvature that substantially changes global morphology of an inflatable at the meter scale (Inset scale bar: 2 cm; Image scale bar: 15 cm). We propose an inverse design pipeline to yield strain limiter design parameters for an uninflated cylinder such that when inflated, its centerline matches a user-input space curve.

more complex emerging systems, the energetic interplay be- 33
tween locally stretched surface regions may give rise to topog- 34
raphy with applications in mechanical camouflage and precision 35
haptic devices (22, 23), or sinuous 3D curves with applications 36

Significance Statement

Inflatables are ubiquitous. Lightweight, strong, and deployable, they have applications in robotics, structures, medicine, and entertainment. Outfitting cylindrical inflatables with stiffer material patches yields complex and functional 3D shapes upon pressurization. Yet, modeling of discretely-constrained cylindrical inflatables poses a significant challenge due to extreme material and geometric nonlinearities and pressure dynamics. The ability to generate designs for bespoke inflated shapes could enhance their utility, reduce prototype iteration, and yield more performant inflatables. We propose an inverse design method that outputs geometric parameters for patch-clad cylindrical inflatables such that they match target 3D curves. Our approach uses an initial conceptual solution based on curve kinematics to seed a finite element simulation nested within an optimization algorithm, resulting in excellent curve matching.

RB conceived of the idea, conducted experiments, created KSA, and performed FE simulations. SP conducted experiments, performed FE simulations, and implemented the optimization algorithm. BG conducted FE simulations. KB and RK-B oversaw the research. All authors contributed to writing the manuscript.

There are no competing interests to declare.

¹To whom correspondence should be addressed. E-mail: rebecca.kramer at yale.edu

37 in continuum manipulation (24). Localized strain-limiting
 38 entails boundary effects arising from material compliance mis-
 39 match that raise the required fidelity of a model to capture
 40 the deforming inflatable's mechanical response.

41 Finite element (FE) analysis has been shown to reliably
 42 predict the behavior of 3D inflating continua outfitted in dis-
 43 crete strain limiters (25). FE simulation has recently been
 44 used for inverse design using neural networks to produce sur-
 45 faces that inflate to programmed 3D topography (26). Design
 46 strategies reliant entirely on machine learning however suffer
 47 from high computational expense, which can preclude their
 48 unaccompanied implementation in large-scale inverse design
 49 problems or transferability to systems composed of different
 50 materials.

51 Despite recent progress, there is still a dearth of inverse
 52 design models for 3D discretely constrained inflatables, which
 53 acts as a bottleneck to adopting multi-functional soft systems
 54 in critical application spaces. This fact motivates a framework
 55 capable of capturing nuanced mechanics for solution accuracy
 56 yet able to generate conceptual solutions in reduced time.
 57 Here we present such a framework and evaluate it by focusing
 58 on a useful, albeit relatively unexplored case of elongated
 59 inflated cylinders clad in discrete strain-limiting "patches."
 60 The number, dimensions, locations, and orientations of patches
 61 placed on the cylinder may be tuned to coerce myriad space
 62 curves (Fig. 1, SI Video 1), with applications ranging from
 63 shape matching, manipulation, navigation, to self-tying knots.
 64 Our inverse method solves for patch design parameters to be
 65 placed on an uninflated cylinder such that the centerline of
 66 the inflated cylinder closely approximates a user-input space
 67 curve.

68 Starting with a user-input space curve ($\mathcal{C} \in \mathbb{R}^3$), we use
 69 kinematics to generate a conceptual solution for strain limiter
 70 placement and heights on the uninflated geometry. Next, the
 71 conceptual solution seeds an FE simulation nested within an
 72 optimization structure that tunes strain limiter placement and
 73 dimensions. The conceptual solution emerges from a reduced-
 74 order model that provides intuition about the mechanics that
 75 govern elongate hyperelastic inflatables clad in discrete strain
 76 limiters; furthermore, seeding the FE optimization loop with
 77 this conceptual solution reduces the design search space, facil-
 78 itating faster convergence on valid parameters than using FE
 79 alone.

80 Results and Discussion

81 Rectangular strain-limiting patches $i = 1 \dots n$ with dimensions
 82 $H_i \times W_i$ are placed on an undeformed cylindrical inflatable of
 83 length L at positions $[X_i, Y_i]$ (on the developable surface), and
 84 angles with respect to the longitudinal axis Θ_i (Fig. 2). Upon
 85 inflation, the inflatable undergoes large extensional and radial
 86 stretches while the patches influence curvature (κ) and torsion
 87 (τ) of the centerline parameterized by arclength t (See Fig.
 88 S1 for fabrication of inflatables and a typical pressure-volume
 89 curve). Herein we strive to model the relationship between
 90 patch placement and $\kappa(t)$ and $\tau(t)$ to systematically program
 91 curves.

92 The inflation of patch-clad cylindrical inflatables is char-
 93 acterized by multiple snap-through instabilities (Note S1).
 94 The first of these instabilities is associated with the inflatable
 95 reaching a critical pressure and developing an initial bulge
 96 (27). Subsequent snap-troughs arise from overcoming local

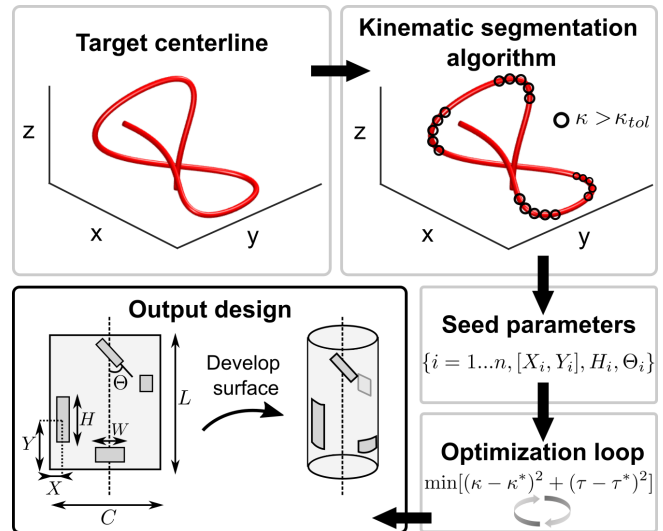


Fig. 2. Visual depiction of inverse design pipeline, starting with a target centerline going into kinematic segmentation algorithm, the solution of which is in turn used to seed a FE simulation nested within an optimization loop. The output of this pipeline are strain limiter design parameters to match a target centerline.

stiffness discontinuities due to the presence of patches (28).
 Once the air bulge has propagated to the cylinder's distal tip,
 the inflatable assumes its fully-inflated shape. This state of
 static equilibrium, in which curvature caused by patches is
 fully "activated," is the concern of the present paper.

Kinematic Segmentation Algorithm. The first part of our in-
 verse design pipeline is a conceptual solution, enabled by a
 reduced-order model, which we dub Kinematic Segmentation
 Algorithm (KSA). Given a target curve \mathcal{C} , KSA quickly gen-
 erates coarse estimates of n , $([X_i, Y_i])$, H_i , and Θ_i along an
 uninflated cylinder, overlooking complexities arising from ma-
 terial properties. The advantage of KSA is twofold: it provides
 insight into the mechanics of the deforming cylinder and an in-
 itial guess for the FE optimization loop to reduce convergence
 time due to the highly non-convex search space.

In KSA, first, a discrete Frenet-Serret triad consisting of the
 tangent \vec{T} , normal \vec{N} , and binormal \vec{B} triad, is calculated for
 \mathcal{C} . We then identify where curvature ($\kappa = ||d\vec{T}/dl||$) exceeds
 a pre-defined threshold κ_{tol} (Note S2). If a point exceeds
 κ_{tol} , we ascribe that point along the arclength to have a patch.
 Close-by segments within a specified tolerance are merged, and
 the axial midpoints of the resulting sections deemed to have a
 patch are calculated, indicating the axial midpoint of a patch in
 the deformed configuration, y_i . Knowing the initial length
 of an uninflated cylinder and the length of a target centerline
 (L_f), we calculate the axial stretch $\lambda = L_f/L$ and then find the
 patch axial midpoint in the reference configuration $Y_i = y_i/\lambda$.
 H_i is estimated as the length of the segments that exceed κ_{tol} .
 We estimate X_i using the angle of twist of \vec{B} along the curve
 up to a midpoint of a segment. Similarly, we estimate Θ_i by
 calculating the angle of twist of \vec{B} through a segment and
 assuming the patch angle in the undeformed configuration maps
 directly to the centerline twist it exerts in the deformed con-
 figuration. Although it rapidly yields a conceptual solution,
 KSA alone does not furnish a complete solution because it does
 not estimate the width of the patches W_i . The influence of
 patch parameters on κ and τ depends on the patch's material

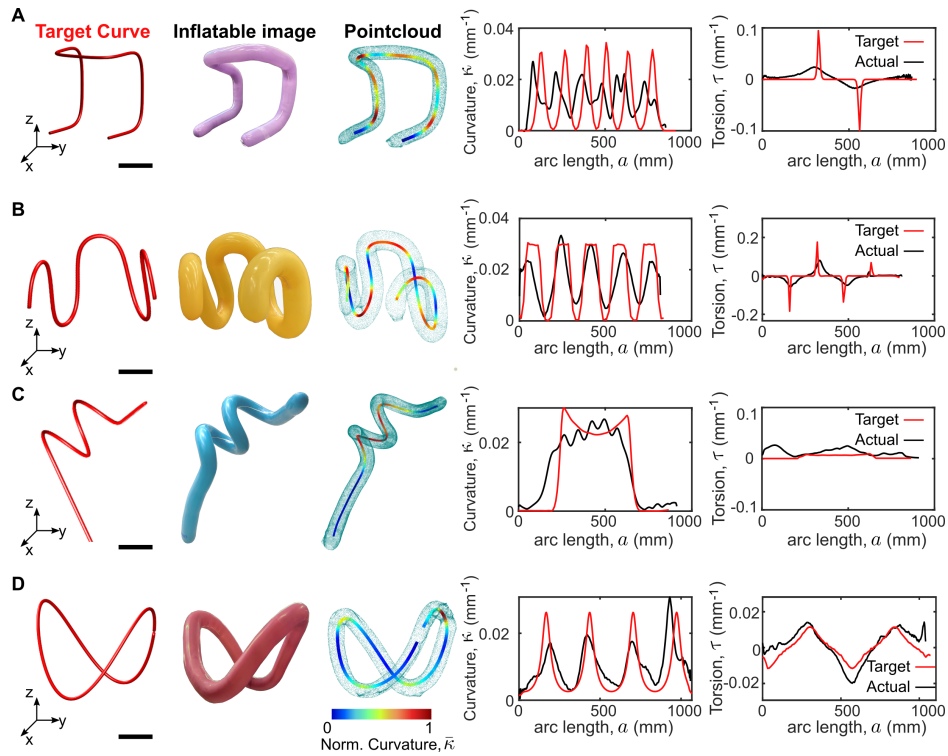


Fig. 3. Benchmark target centerlines used in assessing the KSA-FE optimization pipeline. The curves span a variety of different curvature and torsion profiles as a function of arclength. For each we show the resulting inflatable and a 3D pointcloud of the inflatable with a juxtaposed centerline indicating magnitude of curvature. A. Smooth version of Hilbert's space-filling curve. Scale bar: 8 cm B-C. Hand-drawn curves. Scale bars: 11.5 cm and 7.5 cm, respectively. D. Equation that describes the contour of a hyperbolic paraboloid surface. Scale bar: 10 cm.

134 properties, and the boundary effects between the patch and
 135 the inflated cylinder. Both of these considerations require a
 136 model beyond the simplified kinematic representation.

137 **Finite element model.** An FE simulation nested within an opti-
 138 mization loop constitutes the second part of the inverse design
 139 pipeline. The FE simulations (which were conducted using the
 140 commercial package ABAQUS 2020/Explicit) account for the
 141 mechanical boundary effects and material properties omitted
 142 from KSA through nonlinear elasticity; they model the cylind-
 143 rical inflatable and patches as isotropic membrane elements
 144 governed by hyperelastic constitutive laws (Note S3). We
 145 performed forward validations to ensure the accuracy of the
 146 FE model (Note S4; Fig. S2).

147 In the inverse FE problem, a shape-matching objective is
 148 formulated as a minimization of the squared difference between
 149 target and simulation torsion and curvature:

$$\min_{X_i, Y_i, H_i, W_i, \Theta_i} (\kappa(t) - \kappa(t)^*)^2 + (\tau(t) - \tau(t)^*)^2 \quad [1]$$

$$s.t : Lb_i \leq (X_i, Y_i, H_i, W_i, \Theta_i) \leq Ub_i \quad [2]$$

150 Here, * denotes the target values. An optimal solution is
 151 computed by searching the design space while satisfying the
 152 constraints (bounds on reasonable sizes of patches, denoted
 153 as Lb_i through Ub_i ; see Note S5). Due to the non-convex
 154 search space of the optimization problem and the number of
 155 free variables, we chose an evolutionary algorithm known as
 156 CMA-ES (Co-variance Matrix Adaptation Evolution Strategy),
 157 which is well-suited to such problems (29).

Assessment of inverse design pipeline. We evaluated the in-
 158 verse design pipeline with four input curves (Fig. 3A-D):
 159 Hilbert's space-filling curve (30) (which is not traditionally
 160 differentiable, but we use a smooth approximation), two be-
 161 spoke 3D curves, and an equation-driven curve describing the
 162 contour of a hyperbolic paraboloid (Note S6). We crafted in-
 163 flatables according to the output of the inverse design pipeline
 164 by laser cutting patches and adhering them to the surface of
 165 the inflatable. Then, after inflation, we took a 3D scan of the
 166 inflatable from which the centerline was extracted (Note S7;
 167 Fig. S3).
 168

169 Results testify that the inverse design pipeline can accu-
 170 rately generate valid design parameters to approximate a vari-
 171 ety of space curves with diverse torsion and curvature profiles.
 172 Due to the different lengths of target and experimental cen-
 173 terlines, we used dynamic time warping (31) to quantitatively
 174 evaluate similarity (an explanation of dynamic time warping,
 175 as well as its value for each curve's torsion and curvature as a
 176 function of arclength are tabulated in Note S6). Calculations
 177 yielded a value averaged over all curves of 0.5887 for curvature,
 178 and 1.4899 for torsion.

179 The patch-clad inflatables' successful replication of certain
 180 target curve features, while difficulty in replicating others, elu-
 181 cidates general design considerations for elongate hyperelastic
 182 systems clad in discrete, distributed strain limiters. From the
 183 similarity metric provided by dynamic time warping, we remark
 184 that torsion approximation was less accurate than curvature
 185 approximation. Additionally, sharp peaks in curvature
 186 or torsion over relatively small distances in arclength prove
 187 difficult, owing to the inability of the inflatable to produce

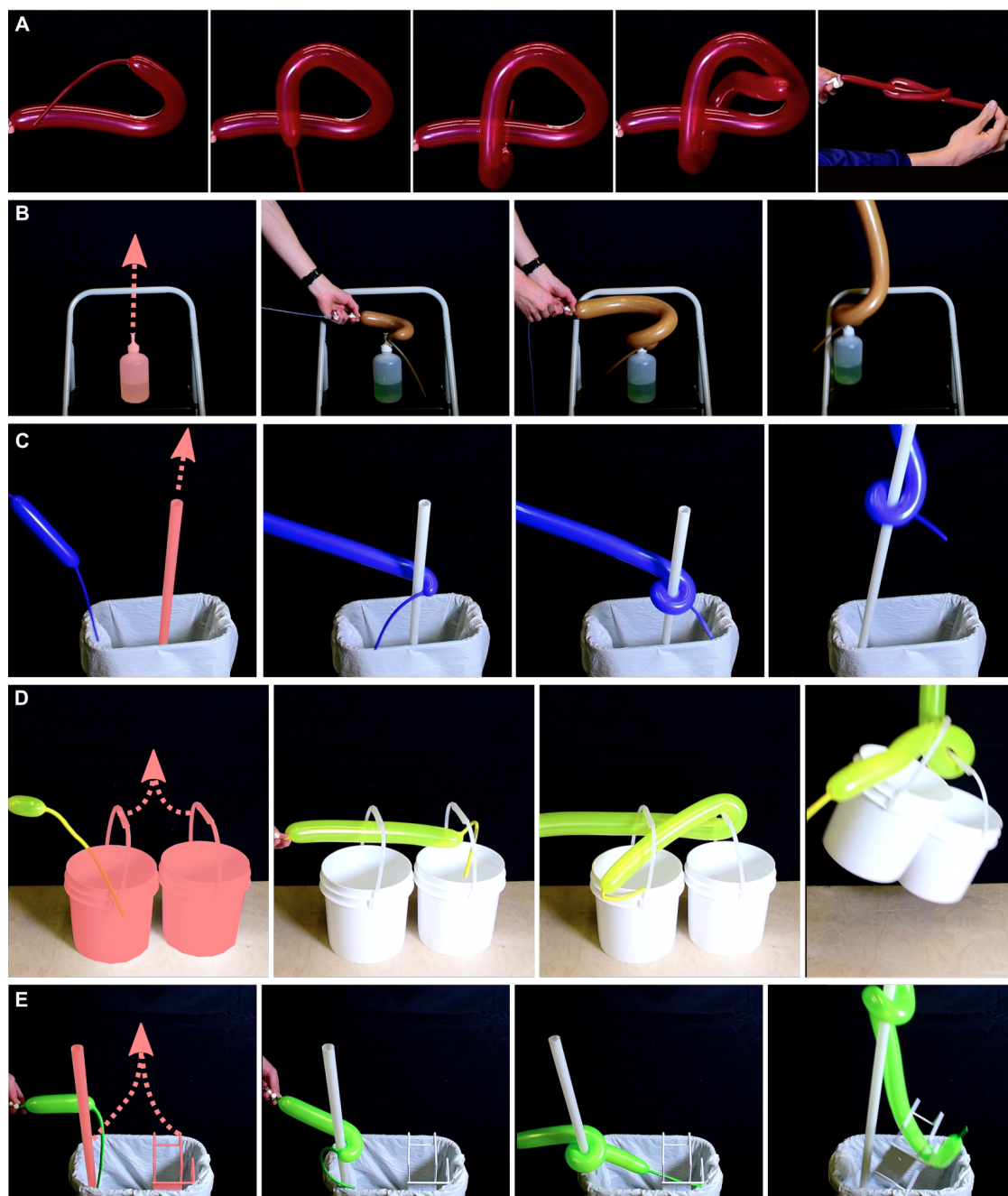


Fig. 4. Applications. A single volumetrically-inflating cylinder clad in discrete strain-limiting patches can accomplish highly dexterous functions. A. Self-tying knot. B. Grasping and lifting a bottle by a 10 mm diameter nozzle using a tight helix. C. Grasping and lifting a PVC pipe of diameter 40 mm using a helix with larger radius. D. Simultaneous grasping and lifting of two buckets by exploiting a loop knot. E. Grasping multiple differently-shaped objects using a combination of enveloping and hinge grasps.

188 true inflection points or twist very rapidly. This challenge is
189 embodied in the Hilbert curve of Fig. 3A, which does not con-
190 sistentlly reach the full extent of target curvature and torsion.
191 Another apparent challenge is maintaining constant κ or τ
192 over a sizable span of arclength. For instance, the inflatable
193 centerline in Fig. 3B does not maintain constant κ at each
194 peak. Likewise, Fig. 3C has small fluctuations in κ that pre-
195 vent it from tracking the smooth dip and rise of the target
196 curve.

197 We ascertained the performance of the FE simulation alone
198 and when it was seeded with KSA in generating designs for
199 Fig. 3C. Results show that KSA generates nearby solution
200 guesses for the patch parameters, limiting the FE search space
201 in the otherwise rugged energy landscape, and reducing the
202 number of required iterations to converge on designs which
203 minimize the objective in equations [1-2] (Note S8; Fig. S4).

204 **Applications.** Equipped with the inverse design framework, we
205 showcase how an inflated shape can be harnessed for robotic
206 functionality beyond mere curve matching. First, we created
207 a self-tying knot (Fig 4A, Video S2), an application necessi-
208 tating both highly curved deformations and non-homogeneous
209 inflation, due to the intersections that are present when map-
210 ping the undeformed to the deformed deformation. Due to
211 a base-to-tip inflation (32), the inflatable experiences no self-
212 intersection until it is deflated and the retraction force tightens
213 the knot. We envision programmable self-tying knots with a
214 single input volume that could be used in medicinal applica-
215 tions, to staunch blood flow, or in deployable structures to
216 rapidly create architectural fixtures.

217 Additionally, we demonstrated programmable grasping of
218 various objects across different length scales using unusual con-
219 tinuum grasp modes (Fig 4B-E, Video S3). Programmed helix
220 diameters or hooking curvatures also enabled the inflatable
221 to manipulate multiple objects at once. For instance, tight
222 helices were able to pinch and lift small-diameter objects, like
223 the nozzle of a soap dispenser (Fig 4B), whereas looser helices
224 served as a power grasp to extract and subsequently return
225 objects of greater diameter, like plastic pipes, in a recycling bin
226 (Fig 4C). Multi-object grasping was accomplished by program-
227 ming distributed functional torsion and curvature across the
228 inflatable length. As examples, with an inflatable consisting of
229 a single volume, we ensnared and lifted two buckets (Fig 4D),
230 or encoded helices and hooks to retrieve disparately-shaped
231 objects—a pipe and a metallic fixture—from a recycling bin
232 (Fig 4E). Ultimately, multiple dissimilar object grasping is vi-
233 able with the elongate inflatables and holds promise for robotic
234 manipulation applications.

235 **Concluding Remarks.** The burgeoning field of soft robotics is
236 rife with soft actuation technologies that expand the bounds
237 of what is possible in robotic functionality. Applying strain
238 limiters to the surface of soft volumetrically-expanding bodies
239 makes it possible to elicit intricate 3D shapes. Despite the
240 ability to easily create them, there is a distinct lack of princi-
241 pled design methods for these highly non-linear soft deforming
242 bodies.

243 With elongate cylindrical systems clad in discrete strain lim-
244 iters as a model system, we present an inverse design method
245 that elicits strain limiter parameters required to match target
246 3D curves. Programming myriad 3D curves is enabled by the
247 proposed modeling pipeline (akin to initial-guess generation

248 techniques (33, 34)) that seeds a high-fidelity FE model with
249 a conceptual solution resulting in a decrease in iterations re-
250 quired to reach desired levels of objective fitness. Moreover,
251 in inverse design, FE can often act as a black box, obfuscating
252 intuition of the design solution (35, 36), which motivates a
253 reduced-order model to provide intuition to the designer. We
254 quantitatively evaluated the efficacy of shape matching with
255 several benchmark curves of varying curvature and torsion
256 profiles, and subsequently demonstrated how inflation to pro-
257 grammed 3D curves can be harnessed to interact dexterously
258 in the environment with a single pressurized volume.

259 There are many exciting avenues related to this study to
260 explore. For instance, a rich design space is available when
261 patch directional moduli are left as a free parameter in the
262 optimization. Novel shapes could be achievable when the
263 patch geometry is not constrained to a rectangle but left to
264 vary. Another remaining challenge is to study how trajectories
265 change under dynamic inflation rather than in quasi-static
266 equilibrium manifolds. Lastly, considering self-contact in the
267 model would expand utility to applications with specified force
268 requirements. In the interest of reducing prototyping time,
269 material waste, and stepping toward optimal performance, we
270 anticipate such an inverse design method could be applied
271 to various other soft systems where modeling has proven a
272 challenge: soft robotics, smart structures, or more generally,
273 any field in which inverse design of 3D inflatables may be
274 applicable.

275 Materials and Methods

276
277 To make strain-limiting patches, Spandex (Polyester Ly-
278 cra/Spandex four-way stretch fabric LY 902, Paylessfabric) was
279 dredged in Liquid Latex (Kangaroo Monster Liquid Latex) and
280 allowed to cure for 24 hr. Patch dimensions were drawn as a DXF
281 file and cut from the spandex composite with a laser cutter (Uni-
282 versal Laser Systems, VLS 2.3). Then, rubber cement (BestTest
283 White Paper Cement, Bestine) served to adhere the patch to the
284 cylindrical inflatable (Qualtex 260d balloons), essentially solvent
285 welding the latex-infused spandex patch to the latex surface. We
286 waited for 24 hr to ensure complete cure and maximum adhesion
287 before inflating. Please see the supporting information for more
288 details about experiments and simulations.

289 **Data Availability.** All data needed to evaluate the conclusions
290 in the paper are present in the paper and/or the Supporting
291 Information. Additional data related to this paper are available
292 from the authors upon request.

293 **ACKNOWLEDGMENTS.** We thank Dr. Gaurav Singh for
294 thought-provoking discussions, and labmates for accommodating
295 guerilla balloon art installations on the benchtops for several months.
296 This project was sponsored by the Office of Naval Research under
297 award N00014-21-1-2417. Any opinions, findings, and conclusions
298 or recommendations expressed in this material are those of the
299 authors and do not necessarily reflect the views of the Office of
300 Naval Research. RB was supported by the NSF Graduate Research
301 Fellowship Program (DGE-1752134)

302 References

- 303 1. E Siéfert, M Warner, Inflationary routes to Gaussian curved topography. *Proc. Royal Soc. A: Math. Phys. Eng. Sci.* **476**, 20200047 (2020). 304
- 305 2. EW Hawkes, LH Blumenschein, JD Greer, AM Okamura, A soft robot that navigates its environment through growth. *Sci. Robotics* **2**, eaan3028 (2017). 306
- 307 3. YJ Kim, S Cheng, S Kim, K Iagnemma, A novel layer jamming mechanism with tunable stiffness capability for minimally invasive surgery. *IEEE Transactions on Robotics* **29**, 1031–1042 (2013). 308 309

- 310 4. E Siéfert, E Reyssat, J Bico, B Roman, Bio-inspired pneumatic shape-morphing elastomers.
311 *Nat. materials* **18**, 24–28 (2019).
- 312 5. D Melancon, B Gorissen, CJ García-Mora, C Hoberman, K Bertoldi, Multistable inflatable
313 origami structures at the metre scale. *Nature* **592**, 545–550 (2021).
- 314 6. AS Gladman, EA Matsumoto, RG Nuzzo, L Mahadevan, JA Lewis, Biomimetic 4d printing.
315 *Nat. materials* **15**, 413–418 (2016).
- 316 7. E Siéfert, E Reyssat, J Bico, B Roman, Programming curvilinear paths of flat inflatables. *Proc.*
317 *Natl. Acad. Sci.* **116**, 16692–16696 (2019).
- 318 8. M Skouras, et al., Designing inflatable structures. *ACM Transactions on Graph.* **33**, 1–10
319 (2014).
- 320 9. J Panetta, et al., Computational inverse design of surface-based inflatables. *ACM Transac-*
321 *tions on Graph.* **40**, 1–14 (2021).
- 322 10. R Baines, S Patiballa, R Kramer-Bottiglio, Rapidly reconfigurable inextensible inflatables in
323 *2021 4th IEEE International Conference on Soft Robotics (RoboSoft)*. (2021).
- 324 11. N El-Atab, et al., Soft Actuators for Soft Robotic Applications: A Review. *Adv. Intell. Syst.* **2**,
325 2000128 (2020).
- 326 12. JC Case, EL White, RK Kramer, Soft Material Characterization for Robotic Applications. *Soft*
327 *Robotics* **2**, 80–87 (2015).
- 328 13. CP Chou, B Hannaford, Measurement and modeling of McKibben pneumatic artificial muscles.
329 *IEEE Transactions on robotics automation* **12**, 90–102 (1996).
- 330 14. F Connolly, CJ Walsh, K Bertoldi, Automatic design of fiber-reinforced soft actuators for tra-
331 jectory matching. *Proc. Natl. Acad. Sci.* **114**, 51–56 (2017).
- 332 15. A Sydney Gladman, EA Matsumoto, RG Nuzzo, L Mahadevan, JA Lewis, Biomimetic 4D
333 printing. *Nat. Mater.* **15**, 413–418 (2016).
- 334 16. L Belding, et al., Slit Tubes for Semisoft Pneumatic Actuators. *Adv. Mater.* **30**, 1704446
335 (2018).
- 336 17. RV Martinez, et al., Robotic tentacles with three-dimensional mobility based on flexible elas-
337 tomers. *Adv. materials* **25**, 205–212 (2013).
- 338 18. J Bishop-Moser, S Kota, Design and Modeling of Generalized Fiber-Reinforced Pneumatic
339 Soft Actuators. *IEEE Transactions on Robotics* **31**, 536–545 (2015).
- 340 19. G Singh, G Krishnan, A constrained maximization formulation to analyze deformation of fiber
341 reinforced elastomeric actuators. *Smart Mater. Struct.* **26**, 065024 (2017).
- 342 20. A Sedal, D Bruder, J Bishop-Moser, R Vasudevan, S Kota, A Continuum Model for Fiber-
343 Reinforced Soft Robot Actuators. *J. Mech. Robotics* **10**, 024501 (2018).
- 344 21. G Singh, G Krishnan, Designing fiber-reinforced soft actuators for planar curvilinear shape
345 matching. *Soft Robotics* **7**, 109–121 (2019).
- 346 22. J Pikul, et al., Stretchable surfaces with programmable 3d texture morphing for synthetic
347 camouflaging skins. *Science* **358**, 210–214 (2017).
- 348 23. WM van Rees, EA Matsumoto, AS Gladman, JA Lewis, L Mahadevan, Mechanics of
349 biomimetic 4d printed structures. *Soft matter* **14**, 8771–8779 (2018).
- 350 24. B Yang, et al., Reprogrammable soft actuation and shape-shifting via tensile jamming. *Sci.*
351 *Adv.* **7**, eabh2073 (2021).
- 352 25. SY Kim, et al., Reconfigurable soft body trajectories using unidirectionally stretchable com-
353 posite laminae. *Nat. communications* **10**, 1–8 (2019).
- 354 26. AE Forte, et al., Inverse Design of Inflatable Soft Membranes Through Machine Learning.
355 *Adv. Funct. Mater.*, 2111610 (2022).
- 356 27. S Kyriakides, C Yu-Chung, The initiation and propagation of a localized instability in an in-
357 flated elastic tube. *Int. J. Solids Struct.* **27**, 1085–1111 (1991).
- 358 28. JTB Overvelde, T Kloek, JJA Dâhaen, K Bertoldi, Amplifying the response of soft actuators
359 by harnessing snap-through instabilities. *Proc. Natl. Acad. Sci.* **112**, 10863–10868 (2015).
- 360 29. N Vasios, AJ Gross, S Soifer, JT Overvelde, K Bertoldi, Harnessing viscous flow to simplify
361 the actuation of fluidic soft robots. *Soft robotics* **7**, 1–9 (2020).
- 362 30. H Sagan, *Space-filling curves*. (Springer), pp. 10–18 (1994).
- 363 31. DJ Berndt, J Clifford, Using dynamic time warping to find patterns in time series in *Pro-*
364 *ceedings of the 3rd International Conference on Knowledge Discovery and Data Mining*,
365 AAAIWS'94. (AAAI Press), p. 359–370 (1994).
- 366 32. I Müller, P Strehlow, *Rubber and rubber balloons: paradigms of thermodynamics*. (Springer
367 Science & Business Media) Vol. 637. (2004).
- 368 33. L Bayón, JM Grau, MM Ruiz, PM Suárez, Initial guess of the solution of dynamic optimization
369 of chemical processes. *J. Math. Chem.* **48**, 28–37 (2010).
- 370 34. P Tsiotras, E Bakolas, Y Zhao, Initial guess generation for aircraft landing trajectory optimiza-
371 tion in *AIAA Guidance, Navigation, and Control Conference*. (2011).
- 372 35. SK Patiballa, G Krishnan, On the design of three-dimensional mechanical metamaterials
373 using load flow visualization. *Mech. Based Des. Struct. Mach.*, 1–26 (2020).
- 374 36. Y Bar-Sinai, G Librandi, K Bertoldi, M Moshe, Geometric charges and nonlinear elasticity of
375 two-dimensional elastic metamaterials. *Proc. Natl. Acad. Sci.* **117**, 10195–10202 (2020).